

Off-shell extrapolation of Regge-model NN -scattering amplitudes describing final-state interactions in ${}^2\text{H}(e, e' p)$

William P. Ford^{1,*} and J. W. Van Orden^{1,2,†}¹*Department of Physics, Old Dominion University, Norfolk, Virginia 23529, USA*²*Jefferson Lab, 12000 Jefferson Avenue, Newport News, Virginia 23606, USA*

(Received 1 July 2013; published 25 November 2013)

In this paper, an off-shell extrapolation is proposed for the Regge-model NN amplitudes presented in a paper by Ford and Van Orden [Phys. Rev. C **87**, 014004 (2013)] and in an eprint by Ford (arXiv:1310.0871 [nucl-th]). A prescription for extrapolating these amplitudes for one nucleon off-shell in the initial state is given. Application of these amplitudes to calculations of deuteron electrodisintegration is presented and compared to the limited available precision data in the kinematical region covered by the Regge model.

DOI: 10.1103/PhysRevC.88.054004

PACS number(s): 25.30.Fj, 24.10.Jv, 21.45.-v

I. INTRODUCTION

Deuteron electrodisintegration experiments have been performed at Jefferson Lab that produce a final proton-neutron state with relatively large invariant masses. Theoretically, the descriptions of these data pose considerable difficulty. At invariant masses below pion production threshold, this reaction can be calculated consistently with potential or meson exchange models. Describing the reaction above pion threshold can be very challenging since it is necessary to include contributions from the open inelastic channels as intermediate states to the observed exclusive pn final state. This means that in principle contributions from electroproduction of mesons, and from the production of mesons and nucleon resonances by pn need to be included for invariant masses above threshold.

The most successful attempt to describe NN scattering above pion threshold was presented in Refs. [1–3]. This paper provides a reasonable description of the NN phase shifts and inelasticities up to a laboratory kinetic energy $T_{\text{lab}} = 1$ GeV ($s = 4m^2 + 2mT_{\text{lab}}$) by including $N\Delta$ and $\Delta\Delta$ intermediate states in a meson-exchange model based on a three-dimensional reduction of the Bethe-Salpeter equation. However, this is at the bottom end of the energy range of the Regge-model fits, and the computer code necessary to obtain off-shell contributions is no longer available. A more recent work [4] extended this model by including $N^*(1440)$ and $N^*(1525)$ resonances and shows calculations up to $T_{\text{lab}} = 1.5$ GeV. However, the total inelastic cross section is much too low for energies much above threshold. It should be emphasized that this is a very difficult problem since the number of pions that can be produced in intermediate states increases significantly with the energy.

In the absence of a consistent dynamical model for use at large invariant masses, it has been common to use the on-shell data to parametrize the final state interaction in calculations of $d(e, e' p)$ above pion threshold. The most common approach has been to use only the central part of a two-dimensional spinor representation of the NN amplitudes parameterized in

terms of the total cross section, the ratio of real to imaginary parts of the forward scattering amplitude, and a parameter for the exponential falloff of the differential cross section as a function of the square of the center-of-mass momentum transfer [5,6]. In Refs. [7–9] we included the full spin-dependence of the np amplitudes by means of constructing Fermi invariants from the scattering analysis interactive dial-in (SAID) helicity amplitudes [10,11] which are available up to $T_{\text{lab}} = 1.3$ GeV. In Ref. [12] the spin dependence is introduced by using the two-dimensional Saclay parametrization of the on-shell amplitudes obtained from SAID up to $T_{\text{lab}} = 1.3$ GeV and the simple parametrization of the central contribution above this energy. In Ref. [6] it is argued that the $d(e, e' p)$ amplitudes will be dominated by on-shell nucleon propagation near $x = 1$. Attempts to estimate off-shell contributions have been introduced in Refs. [7–9] and [12] by introducing prescriptions for the off-shell behavior of the amplitudes along with a cutoff function. These prescriptions are essentially arbitrary. A unique determination of the off-shell behavior the NN amplitudes requires a dynamical model which produces the off-shell values of the scattering amplitudes as an intrinsic part of its solution.

In a recent paper [13] we described a fit to nucleon-nucleon scattering for Mandelstam $s = 5.4$ to $s = 4000$ GeV² using a Regge model. The immediate purpose of this model was to allow extension of calculations of deuteron electrodisintegration to higher invariant masses than was possible using the SAID helicity amplitudes as used in Refs. [7–9]. In Ref. [7] the electrodisintegration amplitude for the $d(e, e' p)$ amplitude for large energy and momentum transfers was described by the Feynman diagram represented in Fig. 1. Diagram Fig. 1(a) represents the plane-wave (PWIA) contribution, while the diagram represented by Fig. 1(b) includes the final-state interaction (FSI). It was shown that the FSI contribution Fig. 1(b) could be represented by the diagrams of Fig. 2. Examination of the poles in the loop integral shows that the integral is dominated by the pole in the propagator for particle 2 which is represented by the cross on this line in diagrams Fig. 2(a)–2(c). The propagator for k'_1 can be separated into an on-shell part Fig. 2(a), an off-shell part with positive energy projection Fig. 2(b), and an off-shell part with negative energy projection Fig. 2(c).

*wpford@jlab.org

†vanorden@jlab.org

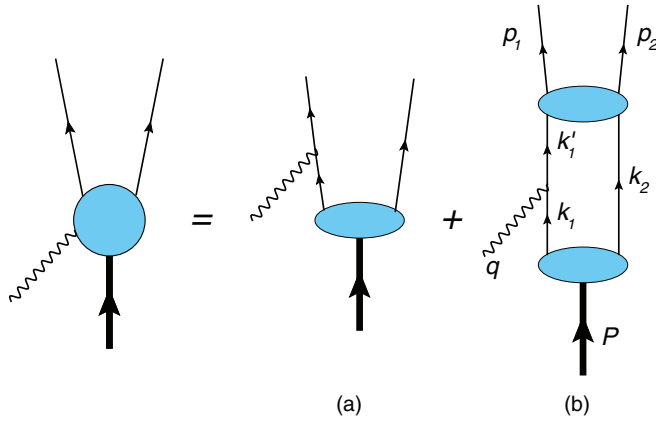


FIG. 1. (Color online) Diagrams representing impulse approximation to deuteron electrodisintegration at large energy and momentum transfers. Diagram (a) is the plane-wave contribution and diagram (b) includes final-state interactions (FSI).

In Ref. [14] we presented a comparison of the FSI contributions to the $d(e, e'p)$ reaction using the SAID and Regge parametrizations of the FSI. Since both the SAID and Regge helicity amplitudes are fit to on-shell data, only the on-shell contribution to the FSI represented by Fig. 2(a) was included. In order to understand the uncertainty in these calculations, it is necessary to have some reasonable estimate of the NN scattering amplitudes off-shell. Working directly with on-shell amplitudes, the amplitudes are functions of s and t only since the crossed diagrams required by Pauli symmetry are included with the on-shell value $u = 4m^2 - s - t$. This constraint is valid only on-shell and the inability to separate the direct and crossed contributions eliminates the possibility of extrapolating the amplitudes off-shell in reasonable manner. The Regge parametrization provides direct contribution as functions of s and t , and the crossed contributions as functions of s and u allowing for the off-shell constraint on the Mandelstam variables to be implemented.

The object of this paper is to provide a reasonable extrapolation of the Regge-model amplitudes for particle 1 off-shell. In Sec. II we will show how this extrapolation is

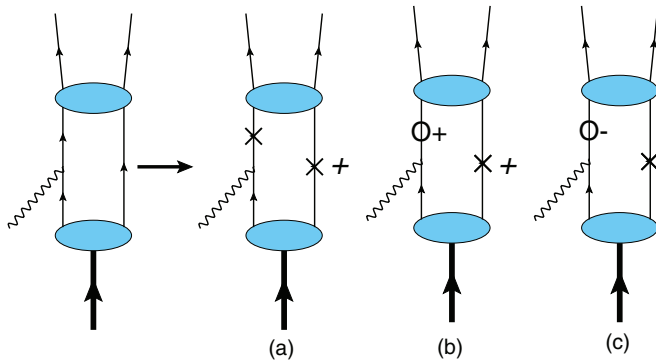


FIG. 2. (Color online) Diagrams representing the separation of the FSI contribution to deuteron electrodisintegration into (a) on-shell, (b) positive energy off-shell, and (c) negative energy off-shell contributions. Diagram (c) gives a small contribution and is neglected in the calculations presented here.

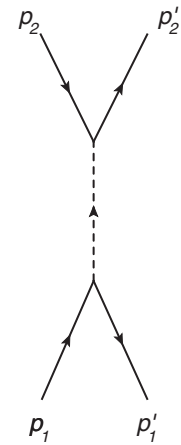


FIG. 3. Representation of the direct contribution to NN scattering through a single meson exchange in the t -channel center of momentum frame.

constructed and show the effects of an off-shell extrapolation of the NN differential cross section. In Sec. III we will apply this off-shell extrapolation to the $d(e, e'p)$ reaction and show its cutoff dependence. Section IV will contain a summary and conclusions drawn from this paper.

II. OFF-SHELL EXTRAPOLATION OF THE REGGE-MODEL NN AMPLITUDES

As described in Refs. [13,14,16], the scattering amplitudes in the s channel are described by Regge exchange in the t channel. In the t -channel center-of-momentum (c.m.) frame the amplitudes are given by NN scattering as represented by Fig. 3. For p_1 off-shell and all other legs on-shell, the four-momenta are given by

$$\begin{aligned} p_1 &= (p_1^0, \mathbf{p}), & p_1' &= (E_t, -\mathbf{p}), \\ p_2 &= (E_t', -\mathbf{p}'), & p_2' &= (E_t', \mathbf{p}'), \end{aligned} \quad (1)$$

where E_t' is the on-shell energy of the final-state particles, $\pm \mathbf{p}'$ are the momenta of the final state particles, E_t is the on-shell energy for initial state particles of momentum $\pm \mathbf{p}$, and p_1^0 is the off-shell energy of particle 1. Using energy conservation, it can be easily shown that

$$\begin{aligned} E_t' &= \frac{\sqrt{t}}{2}, & |\mathbf{p}'| &= \sqrt{\frac{t}{4} - m^2}, \\ E_t &= \frac{t - v}{2\sqrt{t}}, & |\mathbf{p}| &= \sqrt{\frac{(t - v)^2}{4t} - m^2}, \end{aligned} \quad (2)$$

where

$$v = p_1^2 - m^2 \quad (3)$$

is a measure of the off-shellness of particle 1 and m is the nucleon mass. The scattering angle in the t c.m. frame is

$$z = \cos \theta_t = \frac{2s + t - 4m^2 - v}{\sqrt{(4m^2 - t)(4m^2 - \frac{(t-v)^2}{t})}}. \quad (4)$$

For this situation the constraint on the Mandelstam variables s , t , and u is given by

$$s + t + u = 3m^2 + p_1^2 = 4m^2 + v. \quad (5)$$

In Ref. [13] we used helicity matrix elements of the Fermi invariant representation to relate the scalar functions in the Fermi invariant representation to the Reggeized matrix elements in the t c.m. frame. This approach greatly simplifies the analytic continuation of the scattering amplitudes to the physical s c.m. frame. For on-shell scattering there are five terms in the Fermi invariant description of the scattering matrix characterized by the scalar functions \mathcal{F}_S , \mathcal{F}_V , \mathcal{F}_T , \mathcal{F}_P , and \mathcal{F}_A . If p_1 is off-shell, there are five additional scalar functions \mathcal{F}_{S0} , \mathcal{F}_{V0} , \mathcal{F}_{T0} , \mathcal{F}_{P0} , and \mathcal{F}_{A0} . The Fermi-invariant representation of the off-shell scattering operator can then be written as

$$\begin{aligned} \hat{M} = & \mathcal{F}_S(s, t, v) 1^{(1)} 1^{(2)} + \mathcal{F}_V(s, t, v) \gamma^{\mu(1)} \gamma_\mu^{(2)} \\ & + \mathcal{F}_T(s, t, v) \sigma^{\mu\nu(1)} \sigma_{\mu\nu}^{(2)} - \mathcal{F}_P(s, t, v) (i\gamma_5)^{(1)} (i\gamma_5)^{(2)} \\ & + \mathcal{F}_A(s, t, v) (\gamma_5 \gamma^\mu)^{(1)} (\gamma_5 \gamma_\mu)^{(2)} + (\mathcal{F}_{S0}(s, t, v) 1^{(1)} 1^{(2)} \\ & + \mathcal{F}_{V0}(s, t, v) \gamma^{\mu(1)} \gamma_\mu^{(2)} + \mathcal{F}_{T0}(s, t, v) \sigma^{\mu\nu(1)} \sigma_{\mu\nu}^{(2)} \\ & - \mathcal{F}_{P0}(s, t, v) (i\gamma_5)^{(1)} (i\gamma_5)^{(2)} \\ & + \mathcal{F}_{A0}(s, t, v) (\gamma_5 \gamma^\mu)^{(1)} (\gamma_5 \gamma_\mu)^{(2)}) \frac{S^{(1)-1}(p_1)}{2m}, \end{aligned} \quad (6)$$

where

$$S^{(1)-1}(p_1) = \gamma^{(1)} \cdot p_1 - m \quad (7)$$

is the inverse of the propagator with four-momentum p_1 .

The effect of this on a positive-energy spinor is

$$\begin{aligned} & \frac{S^{(1)-1}(p_1)}{2m} u(\mathbf{p}_1, \lambda_1) \\ &= \frac{\gamma^{(1)0} p_1^0 - \boldsymbol{\gamma}^{(1)} \cdot \mathbf{p}_1 - m}{2m} u(\mathbf{p}_1, \lambda_1) \\ &= \frac{\gamma^{(1)0} p_1^0 - \gamma^{(1)0} E_{p_1} + \gamma^{(1)0} E_{p_1} - \boldsymbol{\gamma}^{(1)} \cdot \mathbf{p}_1 - m}{2m} u(\mathbf{p}_1, \lambda_1) \\ &= \left(\frac{\gamma^{(1)0} (p_1^0 - E_{p_1})}{2m} - \Lambda^{(1)-}(\mathbf{p}_1) \right) u(\mathbf{p}_1, \lambda_1) \\ &= \frac{\gamma^{(1)0} (p_1^0 - E_{p_1})}{2m} u(\mathbf{p}_1, \lambda_1) = \frac{v}{2m\sqrt{t}} \gamma^{(1)0} u(\mathbf{p}_1, \lambda_1), \end{aligned} \quad (8)$$

where $E_{p_1} = E_t$ is the on-shell energy of the spinor. Since this is linear in v , the five off-shell terms must vanish on-shell as expected. In addition, while the helicity matrix elements needed to obtain the terms containing \mathcal{F}_i are such that $\lambda_1 = \lambda'_1$ and $\lambda_2 = \lambda'_2$, or $\lambda_1 = -\lambda'_1$ and $\lambda_2 = -\lambda'_2$, the terms containing \mathcal{F}_{i0} require matrix elements where $\lambda_1 = -\lambda'_1$ and $\lambda_2 = \lambda'_2$, or $\lambda_1 = \lambda'_1$ and $\lambda_2 = -\lambda'_2$ due to the extra factor of $\gamma^{(1)0}$. The latter terms are then disjoint from the former, and can not be obtainable from on-mass-shell data.

The actual fitting of the Fermi invariants takes place in the s c.m. frame. In Eq. (6), it is necessary to fit ten scalar functions, while on-shell there are only five helicity matrix elements which are determined on-shell. Consider, for example, that it were possible to construct a model for larger energies based on iteration of an interaction kernel using the spectator equation

[15], which is a three-dimensional reduction of the Bethe-Salpeter equation. A set of coupled integral equations could be written for the helicity amplitudes

$$\begin{aligned} & M_{\lambda'_1, \lambda'_2; \lambda_1, \lambda_2}^+ \\ &= \bar{u}^{(1)}(\mathbf{p}'_1, \lambda'_1) \bar{u}^{(2)}(\mathbf{p}'_2, \lambda'_2) \hat{M} u^{(1)}(\mathbf{p}_1, \lambda_1) u^{(2)}(\mathbf{p}_2, \lambda_2), \\ & M_{\lambda'_1, \lambda'_2; \lambda_1, \lambda_2}^- \\ &= \bar{u}^{(1)}(\mathbf{p}'_1, \lambda'_1) \bar{u}^{(2)}(\mathbf{p}'_2, \lambda'_2) \hat{M} v^{(1)}(-\mathbf{p}_1, \lambda_1) u^{(2)}(\mathbf{p}_2, \lambda_2), \end{aligned} \quad (9)$$

where p_1 and p'_1 would have a range of values encompassing both on-shell and off-shell contributions. The results could then be examined for p'_1 fixed on-shell. Fixing p_1 on-shell for $M_{\lambda'_1, \lambda'_2; \lambda_1, \lambda_2}^+$ gives the fully on-shell helicity amplitudes that can be used to fit to data. For p_1 off-shell there are five possible unique helicity combinations each for $M_{\lambda'_1, \lambda'_2; \lambda_1, \lambda_2}^+$ and $M_{\lambda'_1, \lambda'_2; \lambda_1, \lambda_2}^-$ allowing for all of the scalar functions in Eq. (6).

Unfortunately, as discussed above, there are no available models that can be used to fix the off-shell contributions for $T_{\text{lab}} > 1$ GeV. We can produce a reasonable procedure for extrapolating the \mathcal{F}_i to off-shell values which are constrained at the on-shell point. The \mathcal{F}_{i0} are completely unconstrained. We could, with some difficulty, use such a model below pion threshold to perform this procedure to obtain some information about the complete off-shell behavior, but we can not be sure that the relationship obtained between on-shell and off-shell contributions will hold at larger energies. Aside from imposing a range of arbitrary, unconstrained prescriptions of the \mathcal{F}_{i0} , we could instead concentrate on the constrained \mathcal{F}_i in order to obtain some sense of the properties of off-shell extrapolations that may provide some understanding of the complete problem. We choose to take the latter course and set

$$\mathcal{F}_{S0} = \mathcal{F}_{V0} = \mathcal{F}_{T0} = \mathcal{F}_{P0} = \mathcal{F}_{A0} = 0 \quad (10)$$

in Eq. (6) for this paper.

Additional problems occur in analytic continuation of the Fermi invariants from the t c.m. frame where $t \geq 4m^2$ and $s \leq 0$ to the s c.m. frame where $t \leq 0$ and $s \geq 4m^2$.

The scattering amplitude in the s -channel c.m. frame is represented by Fig. 4 where

$$\begin{aligned} p_1 &= (p_1^0, \mathbf{p}), & p'_1 &= (E, \mathbf{p}'), \\ p_2 &= (E', -\mathbf{p}), & p'_2 &= (E', -\mathbf{p}'). \end{aligned} \quad (11)$$

As in the previous case E' and E represent on-shell energies and p_1^0 is the off-shell energy of particle 1 in the initial state. From conservation of energy

$$\begin{aligned} E' &= \frac{\sqrt{s}}{2}, & |\mathbf{p}'| &= \sqrt{\frac{s}{4} - m^2}, \\ E &= \frac{s-v}{2\sqrt{s}}, & |\mathbf{p}| &= \sqrt{\frac{(s-v)^2}{4s} - m^2}. \end{aligned} \quad (12)$$

In this frame t is given by

$$t = \frac{4m^2 - s + v + \sqrt{(s-4m^2)\left(\frac{(s-v)^2}{s} - 4m^2\right)} \cos \theta_{\text{cm}}}{2}, \quad (13)$$

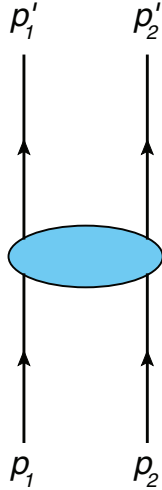


FIG. 4. (Color online) Diagram representing NN scattering in the s channel c.m. frame.

where θ_{cm} is the scattering amplitude in the s c.m. frame. As a result, t is bounded by the functions

$$t_{\text{max}} = \frac{4m^2 - s + v + \sqrt{(s - 4m^2)\left(\frac{(s-v)^2}{s} - 4m^2\right)}}{2} \quad (14)$$

and

$$t_{\text{min}} = \frac{4m^2 - s + v - \sqrt{(s - 4m^2)\left(\frac{(s-v)^2}{s} - 4m^2\right)}}{2}. \quad (15)$$

The maximum value of v is given by

$$v_{\text{max}} = s - 2m\sqrt{s}. \quad (16)$$

These constraints are shown for $s = 7 \text{ GeV}^2$ in Fig. 5, where the physically accessible region is the area between the lines for t_{max} and t_{min} . Note that the on-shell amplitudes are given by $v = 0$ where $t_{\text{max}} = 0$ and $t_{\text{min}} = 4m^2 - s$.

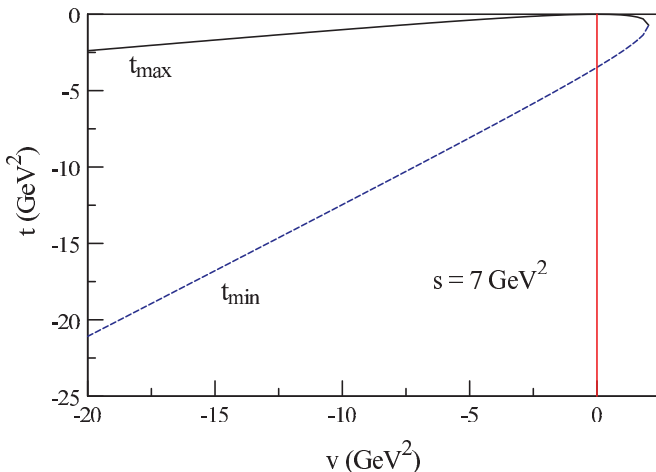


FIG. 5. (Color online) The area between the curve labeled t_{max} and t_{min} contains the allowed values of t in the s c.m. frame as a function of the off-shell parameter v for $s = 7 \text{ GeV}^2$. The line at $v = 0$ shows the range of t for on-shell scattering.

Now consider (4) which gives the value of the t c.m. scattering angle for particle 1 off-shell. Evaluation of z at the extreme values of t in the s c.m. frame gives for $v \neq 0$

$$z(t_{\text{max}})|_{v \neq 0} = z(t_{\text{min}})|_{v \neq 0} = 1. \quad (17)$$

For $v = 0$ we still have,

$$z(t_{\text{min}})|_{v=0} = 1, \quad (18)$$

However,

$$z(t_{\text{max}})|_{v=0} = \frac{s}{2m^2} - 1. \quad (19)$$

So z as described by (4) is discontinuous at $v = 0$. This is a problem for our Regge model parametrization of the scattering amplitudes since the Regge amplitudes are represented as

$$R_{\pm j}^{\text{IPG}}(s, t) \propto \sum_k \xi_{k\pm}(t) \beta_{\pm k}^{\text{IPG}}(t) z^{\alpha_k(t)}, \quad (20)$$

where $\beta^{\text{IPG}}(t) \propto e^{\beta_1 t}$ is the residue, $\xi_{\pm}(t)$ is a phase function, and $\alpha(t) = \alpha_0 + \alpha_1 t$ is the Regge trajectory. The discontinuity in z results in very extreme discontinuous behavior in Regge amplitudes due to the factor of $z^{\alpha(t)}$. This is contrary to the reasonable expectation that the scattering amplitudes should have a smooth continuous extrapolation off-shell. Therefore, a straightforward analytic continuation of the off-shell Fermi invariants for the Regge model from the t c.m. frame to the s c.m. frame is unsatisfactory and an alternate method must be considered.

An alternate approach is to make the off-shell extrapolation after the on-shell Fermi invariants are analytically continued to the s c.m. frame. This requires that we choose a prescription for z off-shell that will be continuous in v . We choose

$$z = \frac{s(t + t_{\text{max}} - 2t_{\text{min}}) - 4m^2(t - t_{\text{min}})}{s(t_{\text{max}} - t) + 4m^2(t - t_{\text{min}})} \quad (21)$$

which is constrained such that

$$z(t_{\text{max}}) = \frac{s}{2m^2} - 1 \quad (22)$$

and

$$z(t_{\text{min}}) = 1 \quad (23)$$

for all allowed values of v .

The remainder of the details of the parametrization follow those in Refs. [13,14,16] and with the exception that Eq. (19) of Ref. [14] is replaced by

$$\begin{aligned} \Xi_{S1}(s, t, v) &= -\frac{m^2}{2(4m^2 - t)}, \\ \Xi_{V2}(s, t, v) &= -\frac{4m^2 - t}{8(2s + t - 4m^2 - v)}, \\ \Xi_{V3}(s, t, v) &= \frac{t}{8(2s + t - 4m^2 - v)}, \\ \Xi_{T3}(s, t, v) &= -\frac{m^2}{4(2s + t - 4m^2 - v)}, \end{aligned}$$

$$\begin{aligned}\mathfrak{E}_{p4}(s, t, v) &= -\frac{m^2}{2t}, \\ \mathfrak{E}_{A5}(s, t, v) &= \frac{1}{8}.\end{aligned}\quad (24)$$

The off-shell cross section

One way to visualize the nature of this off-shell prescription is the calculation of the NN cross section off-shell. The helicity matrix elements of (6) are defined as

$$\begin{aligned}M_{\lambda'_1, \lambda'_2; \lambda_1, \lambda_2}(s, t, v) &= \bar{u}^{(1)}(\mathbf{p}'_1, \lambda'_1) \bar{u}^{(2)}(\mathbf{p}'_2, \lambda'_2) \hat{M}(s, t, v) \\ &\quad \times u^{(1)}(\mathbf{p}_1, \lambda_1) u^{(2)}(\mathbf{p}_2, \lambda_2),\end{aligned}\quad (25)$$

where $u(\mathbf{p}, \lambda)$ is a spinor in the helicity basis. For identical particles, only five amplitudes are independent and are given by

$$\begin{aligned}a(s, t, v) &= \phi_1(s, t, v) = M_{\frac{1}{2}, \frac{1}{2}; \frac{1}{2}, \frac{1}{2}}(s, t, v), \\ b(s, t, v) &= \phi_5(s, t, v) = M_{\frac{1}{2}, \frac{1}{2}; \frac{1}{2}, -\frac{1}{2}}(s, t, v), \\ c(s, t, v) &= \phi_3(s, t, v) = M_{\frac{1}{2}, -\frac{1}{2}; \frac{1}{2}, -\frac{1}{2}}(s, t, v), \\ d(s, t, v) &= \phi_2(s, t, v) = M_{\frac{1}{2}, \frac{1}{2}; -\frac{1}{2}, -\frac{1}{2}}(s, t, v), \\ e(s, t, v) &= \phi_4(s, t, v) = M_{\frac{1}{2}, -\frac{1}{2}; -\frac{1}{2}, \frac{1}{2}}(s, t, v).\end{aligned}\quad (26)$$

A fictitious off-shell c.m. differential cross section can then be defined as

$$\frac{d\sigma}{d\Omega_{\text{cm}}}(s, t, v) = \frac{m^4}{8\pi^2 s} (|a|^2 + 4|b|^2 + |c|^2 + |d|^2 + |e|^2).\quad (27)$$

One source of v dependence in the helicity amplitude results from the matrix elements of the Dirac γ matrices in Eq. (6) using the definitions of the on-shell energies given by (12). In Ref. [7], where the SAID helicity amplitudes were used to describe the FSI, an off-shell prescription was proposed that effectively only contains these contributions. The off-shell c.m. cross sections using the SAID amplitudes for $s = 5.9 \text{ GeV}^2$ are shown in Fig. 6 for pp scattering at various values of v . Here $v = 0$ corresponds to the physical cross section. Note that as the magnitude of v increases the size of the cross section also increases. It can be shown by explicit calculation of the helicity matrix elements using this prescription that the amplitudes must vary as $|v|$ when the magnitude of v becomes large. The cross sections should then vary as v^2 . Clearly, use of this prescription in calculations of deuteron electrodisintegration will diverge unless a cutoff is introduced. In Ref. [7], we introduced a cutoff of the form

$$f(v) = \frac{(\Lambda^2 - m^2)^2}{(\Lambda^2 - m^2)^2 + v^2},\quad (28)$$

where the cutoff mass Λ was typically taken to be 1 GeV.

For the Regge model, the amplitudes (20) depend explicitly on t through the phase factor $\xi(t)$, the Regge trajectory $\alpha(t)$, and the residue factor $\beta^{\text{IPG}}(t) \propto e^{\beta t}$. From Fig. 5 it can be seen that the maximum value of t becomes increasingly negative as v moves away from the on-shell point. This means that the maximum size of the residue factor decreases

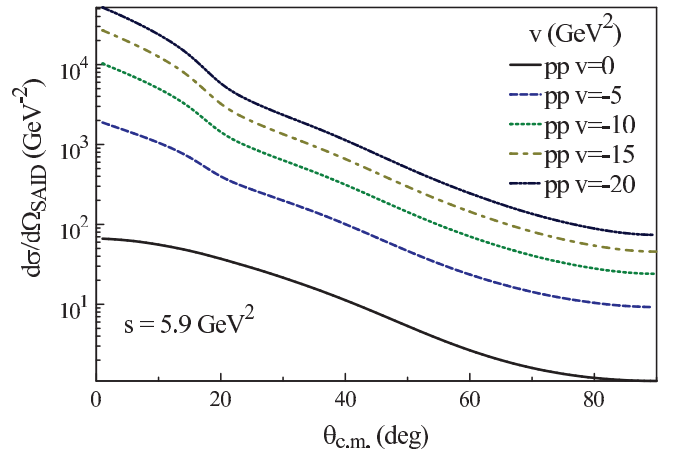


FIG. 6. (Color online) Off-shell cross sections for pp scattering using the SAID helicity amplitudes as a function of v for $s = 5.9 \text{ GeV}^2$.

exponentially away from the on-shell point. In addition, the range of t values that can contribute increases as v becomes more negative. Since the point where the maximum value of u occurs corresponds to the minimum value of t , this causes the overlap of the t and u channel contributions to decrease. We should therefore expect that the off-shell cross sections using the Regge model amplitudes should decrease exponentially as the magnitude of v increases. Figure 7 shows the off-shell pp cross section at $s = 8 \text{ GeV}^2$ for various values of v . This figure shows that the variation of the off-shell cross section with v is consistent with the arguments made above, and decreases exponentially with increasing magnitude of v . The off-shell fall off of the amplitudes is therefore related to the fall off of the on-shell amplitudes with $|t|$ and $|u|$.

III. DEUTERON ELECTRODISINTEGRATION

We now consider the effects of including the off-shell contributions from Fig. 2(b) using the off-shell prescription for the Regge FSI described above. It is useful to include the

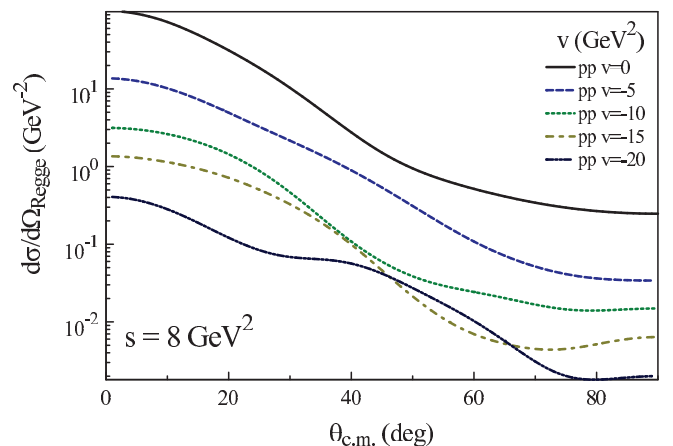


FIG. 7. (Color online) Off-shell cross sections for pp scattering using the Regge amplitudes as a function of v for $s = 8 \text{ GeV}^2$.

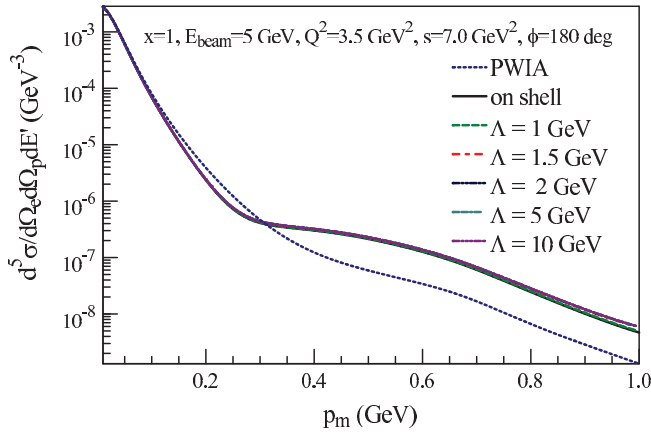


FIG. 8. (Color online) The deuteron electrodisintegration cross section using the Regge FSI for $x = 1$, beam energy $E_{\text{beam}} = 5$ GeV, $Q^2 = 3.5$ GeV 2 , $s = 7.0$ GeV 2 , and $\phi = 180^\circ$.

cutoff (28) as a means of studying the off-shell contributions. Figure 8 shows the differential cross section plotted vs missing momentum p_m for $x = 1$, beam energy $E_{\text{beam}} = 5$ GeV, $Q^2 = 3.5$ GeV 2 , $s = 7.0$ GeV 2 , and $\phi = 180^\circ$. Calculations of the PWIA represented by Fig. 1(a), the PWIA plus the on-shell contribution represented by Fig. 2(a), and the cross section for the PWIA, on-shell and off-shell contributions of Fig. 2(b) for various values of the cutoff mass Λ are shown. It is clear from this figure that at the chosen kinematics the off-shell effects are small. However, since this is a semilog plot, the relative size of the off-shell contributions can be better understood by considering the ratio of off-shell to on-shell cross sections for various values of Λ defined by

$$\sigma_R = \frac{\left(\frac{d^5\sigma}{d\Omega_e d\Omega_p dE'}\right)_\Lambda}{\left(\frac{d^5\sigma}{d\Omega_e d\Omega_p dE'}\right)_{\text{onshell}}} \quad (29)$$

This ratio is shown in Fig. 9 for cutoff masses of 1 to 10 GeV. This shows that the off-shell contribution is quite sensitive to the cutoff mass for values below 2 GeV, but quickly saturates for larger values of the cutoff mass. Indeed the effect

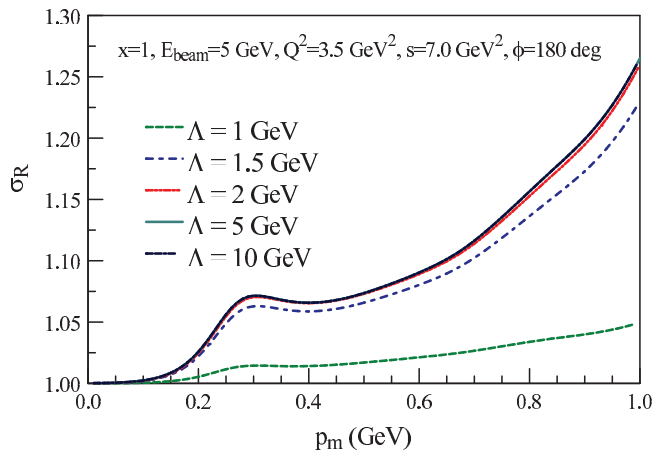


FIG. 9. (Color online) Ratio of off-shell to on-shell cross sections for various values of the cutoff mass.

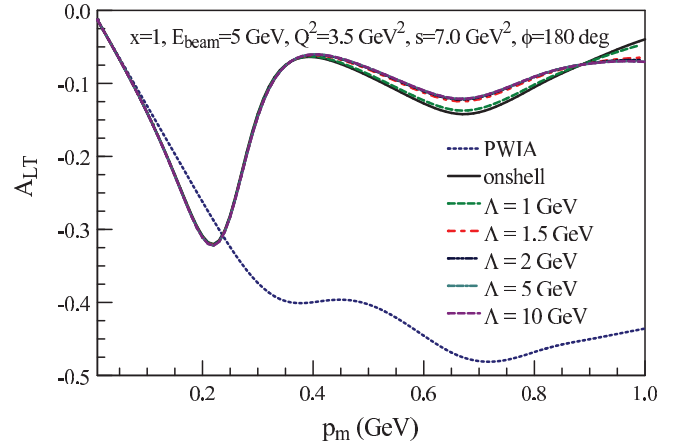


FIG. 10. (Color online) The asymmetry A_{LT} for PWIA, on-shell and off-shell FSI with different cutoff masses.

is effectively saturated by $\Lambda = 10$ GeV, and we will use this value of the cutoff mass to represent the maximum variation in the off-shell contributions in subsequent figures. Note that the size of the off-shell effects increases with increasing missing momentum, and has maximum value for these kinematics of about 25% at $p_m = 1.0$ GeV. The off-shell contributions vary significantly with kinematics and are potentially large.

An example of off-shell contributions to the asymmetry A_{LT} is shown in Fig. 10 for the same kinematics as in the previous figures. For this asymmetry the effect of including the on-shell FSI is large, but the contributions of off-shell scattering is small for these kinematics. As in the case of the cross sections, the rapid saturation of off-shell contributions is evident.

The differential cross section for $x = 1.3$, $E_{\text{beam}} = 12$ GeV, $Q^2 = 7.5$ GeV 2 , $s = 7.54$ GeV 2 , and $\phi = 180^\circ$ is shown in Fig. 11. For these kinematics the on-shell cross section is substantial below the plane-wave cross section. For the $x = 1$ kinematics of Fig. 8, the on-shell cross section is larger than the PWIA cross section. In this case, we show only the case of saturated off-shell contributions with $\Lambda = 10$ GeV. Here the off-shell contributions tend to move the cross section back toward the PWIA for most values of the missing momentum.

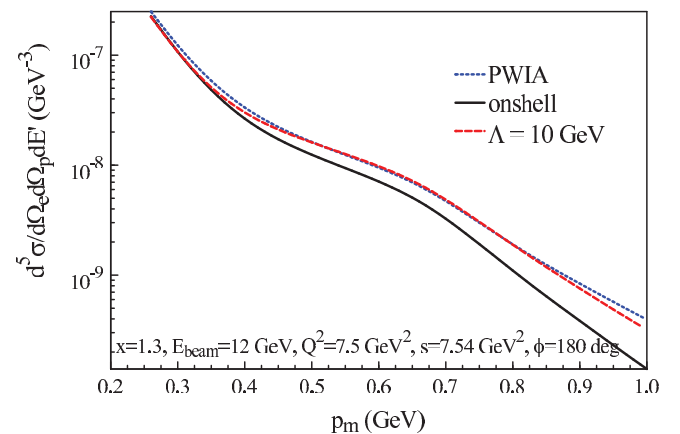


FIG. 11. (Color online) Differential cross section for $x = 1.3$, $E_{\text{beam}} = 12$ GeV, $Q^2 = 7.5$ GeV 2 , $s = 7.54$ GeV 2 , and $\phi = 180^\circ$

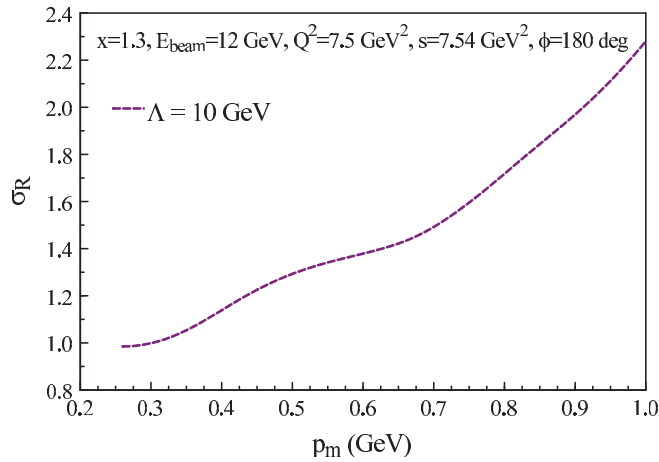


FIG. 12. (Color online) Cross section ratio σ_R for the same kinematics as the previous figure.

The size of this effect can be seen by plotting the ratio of off-shell to on-shell cross sections as shown in Fig. 12. Clearly, for these kinematics the size of the off-shell contributions to the cross section are much larger than for the previous $x = 1$ kinematics. The saturation value at $p_m = 1$ GeV is about 130% above the on-shell contribution as opposed to about 25% of the $x = 1$ kinematics.

Since the off-shell prescription described here is somewhat arbitrary and incomplete, it is necessary to compare the computed cross sections to precision data to determine how large the effect should be. Unfortunately, there is a relatively small amount of data available in the kinematic regions where the Regge-model parametrization applies. The principal source of such data is from [17]. The cross sections in this paper are subdivided into a number of kinematical sets that display a large variation in the values of x and s . In order to allow these to be compared for each of the values of p_m , the cross sections are normalized by the plane-wave calculation performed at

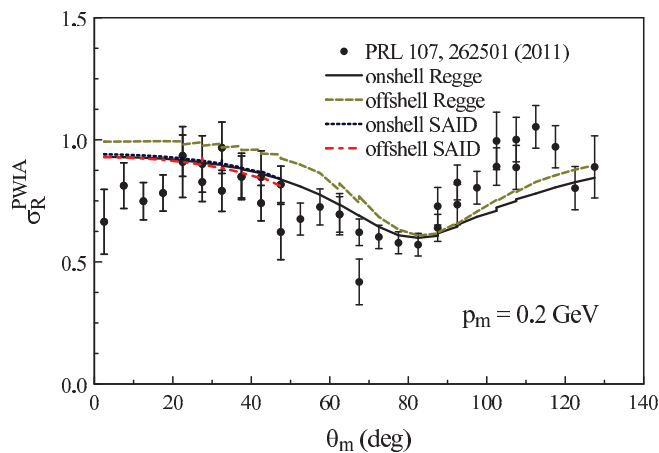


FIG. 13. (Color online) Ratio of FSI cross sections to the PWIA cross section as a function of θ_m for $p_m = 0.2$ GeV. Data are from [17]. $\Lambda_{\text{SAID}} = 1$ GeV, and $\Lambda_{\text{Regge}} = 10$ GeV.

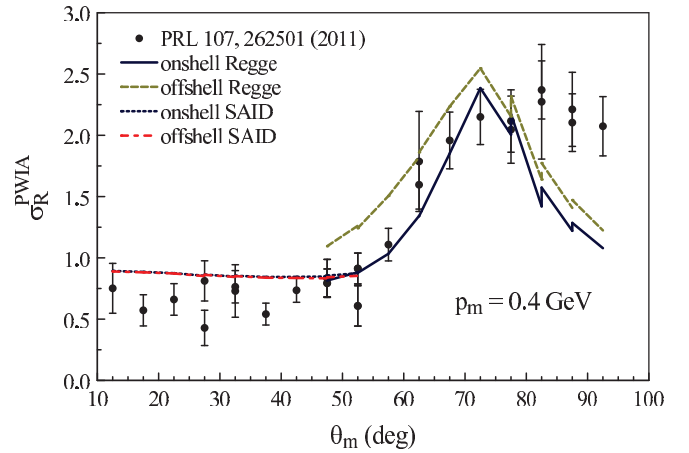


FIG. 14. (Color online) Ratio of FSI cross sections to the PWIA cross section as a function of θ_m for $p_m = 0.4$ GeV. Data are from [17]. $\Lambda_{\text{SAID}} = 1$ GeV, and $\Lambda_{\text{Regge}} = 10$ GeV.

each kinematic point. This is defined by the ratio

$$\sigma_R^{\text{PWIA}} = \frac{\left(\frac{d^5\sigma}{d\Omega_e d\Omega_p dE'}\right)}{\left(\frac{d^5\sigma}{d\Omega_e d\Omega_p dE'}\right)^{\text{PWIA}}}. \quad (30)$$

The data and calculations for this quantity are shown in Fig. 13 for $p_m = 0.2$ GeV, Fig. 14 for $p_m = 0.4$ GeV, and Fig. 15 for $p_m = 0.5$ GeV. For each case four calculations are shown. The calculation labeled “onshell Regge” uses the on-shell contribution from the Regge-model FSI. The calculation labeled “offshell Regge” uses the off-shell Regge-model FSI with $\Lambda = 10$ GeV. The calculation labeled “onshell SAID” uses the on-shell SAID amplitudes and that labeled “offshell SAID” uses the off-shell prescription for the SAID amplitudes with $\Lambda = 1$ GeV. In these figures smaller values of θ_m are associated with large values of x and small values of s , and larger values of θ_m are associated with small values of x and large values of s . Roughly, $0.8 < x < 1.5$ and $4.8 \text{ GeV}^2 < s < 8.5 \text{ GeV}^2$. In all three cases all of the

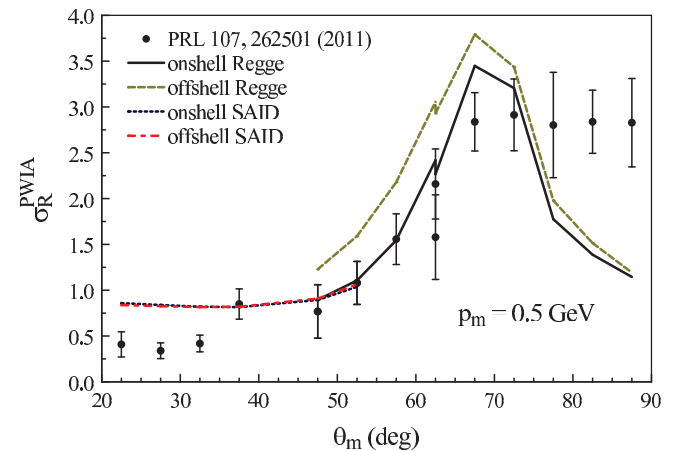


FIG. 15. (Color online) Ratio of FSI cross sections to the PWIA cross section as a function of θ_m for $p_m = 0.5$ GeV. Data are from [17]. $\Lambda_{\text{SAID}} = 1$ GeV, and $\Lambda_{\text{Regge}} = 10$ GeV.

calculations agree qualitatively with shape of the data except at the largest and smallest angles. In regions where the SAID and Regge calculations overlap they are in close agreement. The calculations for the off-shell SAID FSI vary little from the corresponding on-shell results. It should be noted that none of the calculations [5,6,12] shown in Ref. [17] provides a satisfactory description of all of the data.

The calculations containing the off-shell Regge-model FSI along with the corresponding on-shell calculation provides the range of off-shell contributions that can be obtained with the prescription presented in this paper. For all three values of p_m the off-shell calculation is larger than the on-shell calculation. Comparison with the data suggests that the off-shell contributions should be small. It would, however, be prudent to use some caution in accepting this result until more data can be obtained. It should be noted that if the off-shell contributions do indeed prove to be small, this is very advantageous for calculating deuteron electrodisintegration observables for the purposes of simulating potential experiments since the off-shell contributions are much more computationally expensive than are the PWIA and on-shell contributions.

IV. SUMMARY AND CONCLUSIONS

In this paper we have proposed a reasonable estimation of the Regge-model NN scattering amplitude to the case where one of the initial nucleons is off-shell. This extrapolation is smooth and self-regulating. It is shown that the falloff of the off-shell amplitudes is related to the falloff of the on-shell amplitudes with $|t|$ and $|u|$. Application of this approach to deuteron electrodisintegration show that the off-shell contributions are dependent on kinematics and are potentially large. However, comparison to the data from [17] suggest that off-shell effects may be small. Caution should be taken in accepting this result until other data sets may become available.

ACKNOWLEDGMENTS

This work was supported in part by funds provided by the US Department of Energy (DOE) under a cooperative research agreement under Contract No. DE-AC05-84ER40150, and in part by Jefferson Science Associates, LLC, under US DOE Contract No. DE-AC05-06OR23177. The authors would like to thank Werner Boeglin for providing the data presented in this paper.

-
- [1] E. E. van Faassen and J. Tjon, *Phys. Rev. C* **28**, 2354 (1983).
 - [2] E. E. van Faassen and J. A. Tjon, *Phys. Rev. C* **30**, 285 (1984).
 - [3] E. van Faassen and J. A. Tjon, *Phys. Rev. C* **33**, 2105 (1986).
 - [4] EDDA Collaboration, A. Pricking, Ch. Elster, A. Gardestig, and F. Hinterberger, [arXiv:0708.3692](https://arxiv.org/abs/0708.3692) [nucl-th].
 - [5] C. Ciofi degli Atti and L. P. Kaptari, *Phys. Rev. C* **71**, 024005 (2005).
 - [6] J. Laget, *Phys. Lett. B* **609**, 49 (2005).
 - [7] S. Jeschonnek and J. W. Van Orden, *Phys. Rev. C* **78**, 014007 (2008).
 - [8] S. Jeschonnek and J. W. Van Orden, *Phys. Rev. C* **80**, 054001 (2009).
 - [9] S. Jeschonnek and J. W. Van Orden, *Phys. Rev. C* **81**, 014008 (2010).
 - [10] SAID, <http://gwdac.phys.gwu.edu/>, accessed: 2012-09-21.
 - [11] R. A. Arndt, W. J. Briscoe, I. I. Strakovsky, and R. L. Workman, *Phys. Rev. C* **76**, 025209 (2007).
 - [12] M. M. Sargsian, *Phys. Rev. C* **82**, 014612 (2010).
 - [13] W. P. Ford and J. W. Van Orden, *Phys. Rev. C* **87**, 014004 (2013).
 - [14] W. P. Ford, S. Jeschonnek, and J. W. Van Orden, *Phys. Rev. C* **87**, 054006 (2013).
 - [15] F. Gross, J. W. Van Orden, and K. Holinde, *Phys. Rev. C* **45**, 2094 (1992).
 - [16] W. P. Ford, Ph.D. thesis, Old Dominion University, 2013, [arXiv:1310.0871](https://arxiv.org/abs/1310.0871) [nucl-th].
 - [17] W. U. Boeglin *et al.* (Hall A Collaboration), *Phys. Rev. Lett.* **107**, 262501 (2011).